Journal of Photonics for Energy

PhotonicsforEnergy.SPIEDigitalLibrary.org

Effect of particle size distribution on near-field thermal energy transfer within the nanoparticle packings

Anil Yuksel
Edward T. Yu
Michael Cullinan
Jayathi Murthy

SPIE.

Anil Yuksel, Edward T. Yu, Michael Cullinan, Jayathi Murthy, "Effect of particle size distribution on near-field thermal energy transfer within the nanoparticle packings," *J. Photon. Energy* **9**(3), 032707 (2019), doi: 10.1117/1.JPE.9.032707.

Effect of particle size distribution on near-field thermal energy transfer within the nanoparticle packings

Anil Yuksel,[a,*] Edward T. Yu,[b] Michael Cullinan,[a] and Jayathi Murthy[c]
[a]University of Texas at Austin, Department of Mechanical Engineering, Austin, Texas, United States
[b]University of Texas at Austin, Department of Electrical Engineering, Austin, Texas, United States
[c]University of California, Los Angeles, Samueli School of Engineering and Applied Science, Los Angeles, California, United States

Abstract. Nanoscale size effects give rise to near-field thermal considerations when heating nanoparticles under high laser power. We solve Maxwell's equations in the frequency domain to analyze near-field thermal energy effects for three nanoparticle assemblies with different variances in particle sizes and show that heat dissipation generally decreases as the spread in nanoparticle sizes increases within the nanoparticle packing. For this study, log-normally distributed copper nanoparticle packings with a mean radius of 116 nm and three different standard deviations (12, 48, and 84 nm) were created by using a discrete element model in which a specified number of particles is generated. The nanoparticle packings in the simulation are created by randomly placing each nanoparticle into the packing domain with a random initial velocity and a position. The nanoparticles are then allowed to interact with each other under gravitational and weak van der Waals forces until they settle to form a stable packing configuration. A finite-difference frequency-domain analysis, which yields the electromagnetic field distribution, is then applied to the packing by solving Maxwell's equations to obtain absorption, scattering, and extinction coefficients. This analysis is used to calculate the surface plasmon effects due to the electromagnetic coupling between the nanoparticles and the dielectric medium under the different distributions and show that different particle distributions can create different plasmonic effects in the packing domain, which results in nonlocal heat transport. Overall, this analysis helps to reveal how sintering quality can be enhanced by creating stronger laser–particle interactions for specific groups of nanoparticles. [DOI: 10.1117/1.JPE.9.032707]

Keywords: near-field thermal energy transfer; laser heating; light–matter interaction.

Paper 18119SS received Oct. 1, 2018; accepted for publication Dec. 10, 2018; published online Jan. 8, 2019.

1 Introduction

Photonic sintering of nanoparticles is commonly used for the additive manufacturing of printed electronic devices due to its ability to produce high conductivity, microscale structures on a variety of substrates.[1] In this process, light is used to excite the electrons within the nanoparticles causing the nanoparticles to heat up due to resistive heating. This creates a very rapid temperature rise in the nanoparticles and allows them to be sintered in a few milliseconds to form a part. One of the most promising new technologies for the fabrication of three-dimensional (3-D), microelectronic structures is the microscale selective laser sintering (μ-SLS) process. In this process, a thin layer of nanoparticles (<1 μm thick) is spread onto a substrate and then this layer is exposed to high intensity laser light that is patterned using a micromirror array. The light reflecting off the micromirrors is focused so that each mirror has a spot size of ~1 μm. This allows up to 2 million spots to be selectively sintered in the nanoparticle layer simultaneously with a 1-μm resolution. Once the layer is patterned, a new layer of nanoparticles is

*Address all correspondence to Anil Yuksel, E-mail: anil.yuksel@utexas.edu

1947-7988/2019/$25.00 © 2019 SPIE

coated onto the substrate and the selective sintering process is repeated to build up the 3-D microelectronic structures. This process offers the ability to fabricate complex, microscale metal structures at a high rate but generally requires an iterative process of trial-and-error experiments to determine the appropriate processing parameters for any new part. This is because of our lack of understanding of the light–matter interactions within the nanoparticle packing and how these interactions result in heating of the nanoparticles.

One of the greatest sources of uncertainty in this process is the near-field thermal energy transfer within the nanoparticle assemblies. Numerous models of photonic sintering for microscale particles currently exist, but very few models exist for packing scale sintering of nanoparticles. Often for packing-level simulations with microscale particles, these packings are modeled as a continuous medium[2–5] where the heat equation, along with a laser source term, is discretized across the domain using a finite element or finite volume mesh, and the resulting set of algebraic equations is solved to yield a prediction of the temperature distribution in the domain. This type of modeling approach works well when the optical, thermal, and melt/sintering properties of the packing are well known but becomes challenging in nanoparticle packing systems such as the μ-SLS process where the properties of the packing are not well known. Therefore, in nanoparticle-based systems, other methods such as the discrete element method (DEM) are commonly used to estimate the packing properties. DEM is a versatile technique for modeling particle packings where each particle in a domain is represented as a sphere with a specified temperature, conductivity, specific heat, and emissivity.

Numerous models have been developed to predict the optical and thermal[6–9] properties of macroscale SLS nanoparticle packings, but few models exist for the microscale process due to the fact that the physics of the photonic sintering process changes as the particles in the nanoparticle packing become smaller than the wavelength of light used to sinter them. For example, the optical reflectivity and absorption of the nanoparticle packing are strongly influenced by the type of nanoparticle, size, and interparticle spacing[10] due to the wave nature of light at the nanoscale. In addition, metal nanoparticles show unique plasmonic behavior under light illumination at particular wavelengths, which makes them particularly sensitive to the illumination and packing structure.[11] Therefore, new models need to be developed for packing-scale nanoparticle sintering processes such as the μ-SLS process.

This paper presents optical and thermal modeling of a 1 μm $\times$ 1 μm nanoparticle packing that has been generated using copper nanoparticles with 116-nm mean radius and three different standard deviations. Simulation of the large-scale nanoparticle packing is important because previous results have shown that the orientation and spacing between copper nanoparticles can have a significant effect on the optothermal properties of the nanoparticle assemblies,[12,13] and the spacing and orientation of the particles in the nanoparticle packing is greatly influenced by the initial conditions created during the formation of the nanoparticle packing.[14] Ultimately, the results from this analysis will be used to make predictions of the packing temperature and give insights into part formation in processes that utilize the photonic sintering of large numbers of nanoparticles to create parts.

2 Modeling Setup

In this paper, Maxwell's equations are solved for various packing configurations using finite-difference frequency-domain simulations. This is done in order to analyze the effect of the variance in the size of the nanoparticles on the near-field electromagnetic field intensity and the heat generated in the nanoparticle packing. In these simulations, the light from the laser is modeled as an incident plane wave and the scattering from nanoparticles in the packing acts to cause a perturbation to the field induced by this plane wave. The total wave can be expressed as the superposition of the incident wave, a reflected wave in the domain, and a transmitted wave in the substrate. Because the scatterers are placed on a substrate, Maxwell's full field equation is solved first without the presence of the scatterers; this simulation provides the entering background field to the domain for the scattered field analysis. To achieve this, one port in the simulation is set up ($E_0 = 1$ V/m) to define the incident plane wave and the other port is set up to absorb the transmitted wave. Floquet boundary condition is applied as a periodic boundary condition for

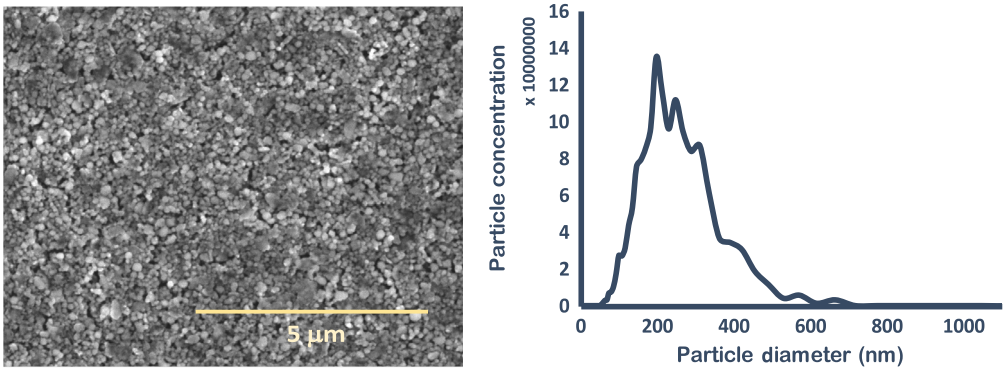

Fig. 1 (a) SEM image of a nanoparticle packing with log-normally distributed copper nanoparticles that have 116-nm mean radius and 48-nm standard deviation and (b) particle size distribution measured using dynamic light scattering.

1×1 μm unit cell. The complex permittivity function of the metallic nanoparticles is taken from Johnson and Christy,[15] and the nanoparticles are placed onto a 350-nm thick, glass substrate with a refractive index of 1.5 and are surrounded by air with a refractive index of 1. A 532-nm, TE (y-polarized) plane wave, which is also shown in Fig. 3(b), is used as the laser illumination source for the simulations in this paper because it is the laser source most commonly used in the experimental studies of laser sintering of metal nanoparticles.[16,17] The scattering cross-sections of the packings are found by calculating the surface integral of the scattered Poynting vector and the absorption cross-sections are found by calculating the volume integral of the energy absorbing by the nanoparticles. Heat dissipation is also found by the multiplication of calculated absorption cross-section and the incident laser power.

Figure 1 shows a scanning electron micrograph of a copper nanoparticle distribution in a nanoparticle packing. Using dynamic light scattering, the copper nanoparticles were measured to have a log-normal distribution with a mean radius of 116 nm and a standard deviation of 48 nm. In order to understand the effect of the variation in the particle size distribution on the optothermal properties of the packings, three different DEM simulations were set up using log-normal particle size distributions with a mean particle radius of 116 nm and standard deviations of 12, 48, and 84 nm, respectively. Figure 2 shows the three particle size distributions generated by DEM within $1 \times 1 \times 1$ μm unit cells used in this study. Previous work has shown that the formation of these nanoparticle packings can accurately be modeled using only weak van der Waals (vdW) forces and gravitational forces to drive the settling of the nanoparticles into stable packing configurations.[14] Hence, the nanoparticle packings for this study were generated

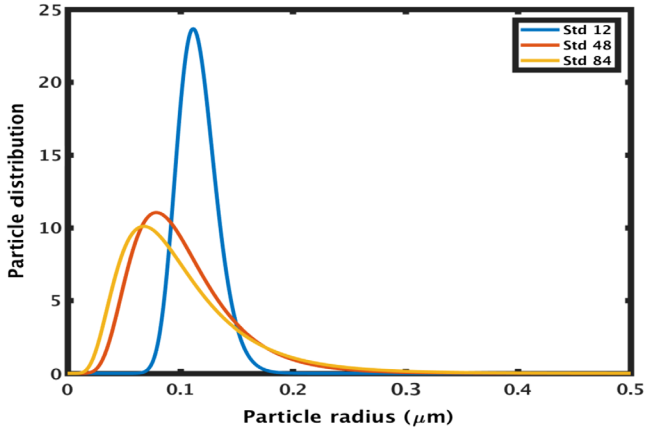

Fig. 2 Log-normal particle distributions at 116-nm mean radius with different standard deviations.

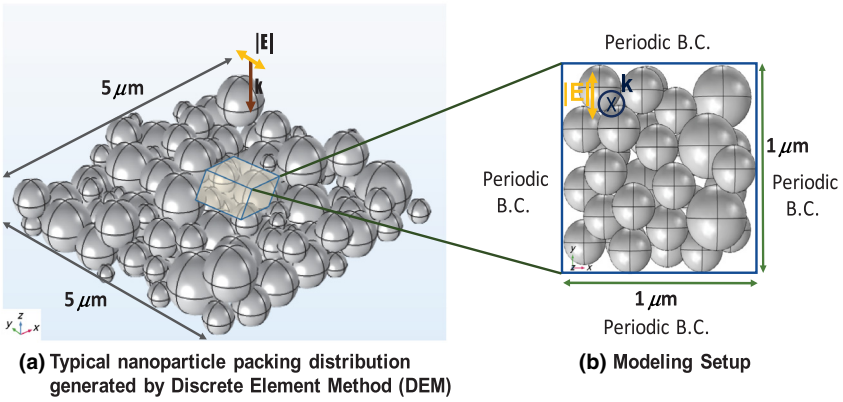

Fig. 3 Modeling analysis geometry.

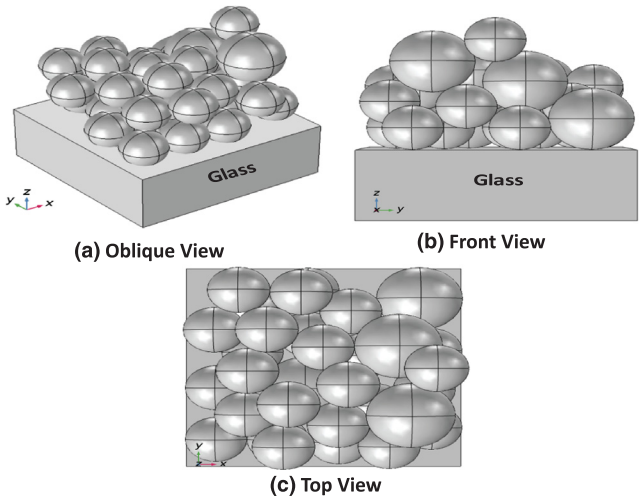

Fig. 4 Log-normal particle distribution with standard deviation 12 nm.

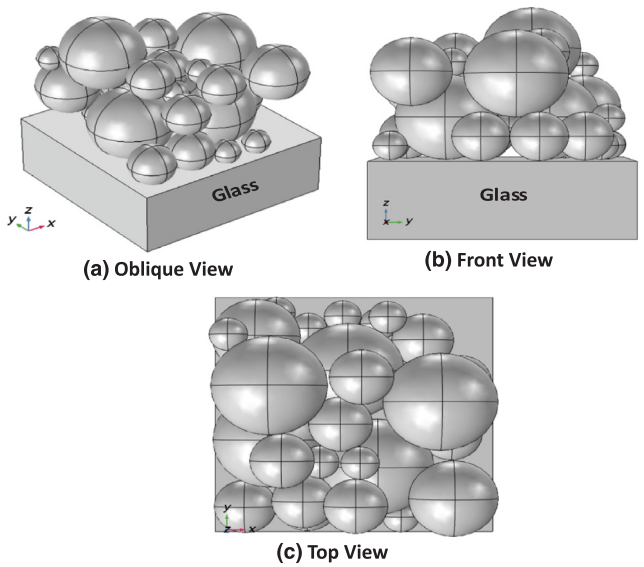

Fig. 5 Log-normal particle distribution with standard deviation 48 nm.

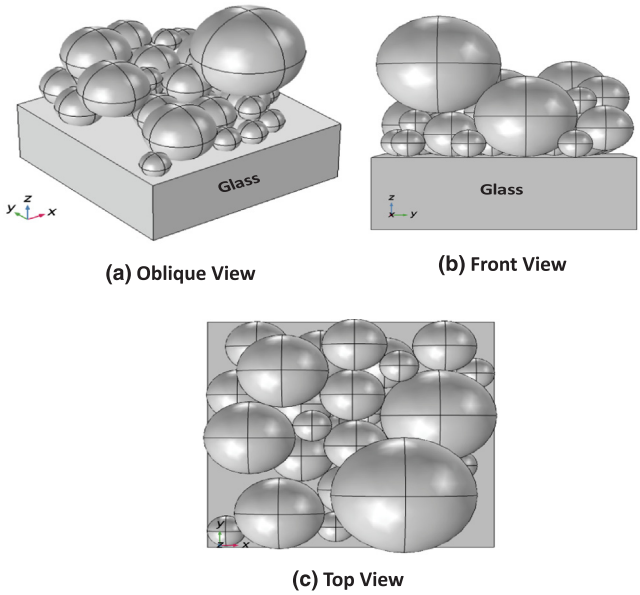

Fig. 6 Log-normal particle distribution with standard deviation 84 nm.

by applying only weak vdW and gravitational forces to the DEM simulations for each of the different particle size distributions selected. The detailed model setup is shown in Fig. 3.

Figures 4–6 show the specific log-normally copper nanoparticle packings with standard deviations of 12, 48, and 84 nm, respectively. The nanoparticle packings all have the same 116-nm mean particle radius.

3 Results and Discussion

The nanoparticle packing distributions can be seen in Figs. 4–6 to differ significantly for different standard deviations. This is mainly due to the effect that vdW forces have on the packing formation process since smaller nanoparticles are subject to greater vdW forces and, therefore, tend to agglomerate more than the bigger nanoparticles. Overall, as the particle size distribution gets wider, the agglomeration increases due to the presence of more very small nanoparticles. This results in a less even spacing of nanoparticles as the particle size standard deviation increases and causes the packings to exhibit different plasmonic behaviors. For example, agglomeration can result in nanoparticle chains where collective plasmonic modes can occur. In fact, previous work[11] has shown that collective plasmonic modes can result in very high field enhancements on clustered nanoparticle packings in air medium, implying very intense heat flux transfer between the nanoparticles clusters. Also, the propagation length of the plasmon modes and the penetration depth have been shown to be affected by the particle size and the particle spatial arrangement in the nanoparticle assembly.[18]

This study investigates the effect of the packing configuration on the energy flux density (W/m^2) at different locations above the glass substrate, where the distance z represents the distance above the glass substrate, by calculating the time-averaged Poynting vector for each of the packing configurations when exposed to TE (Y-pol.) polarized light. As can be observed in Figs. 7–9, the particle size and spacing between particles can have a very large effect on the local energy flux density due to local field enhancements that can create very intense hotspots within the particle packings. In addition, the instantaneous energy flow within the packings tends to be in the direction of the polarization, as should be expected.

For the 12-nm standard deviation case shown in Fig. 7, a cluster of nanoparticles can be observed at around 100 nm above the glass substrate. This clustering leads to enhanced plasmonic behavior between the particles as can be observed in Fig. 7(b). This enhanced plasmonic behavior is due to the collective plasmonic modes, which span three or more particles aligned in a chain-like arrangement,[19–21] that are coupled by the near-field interactions between the

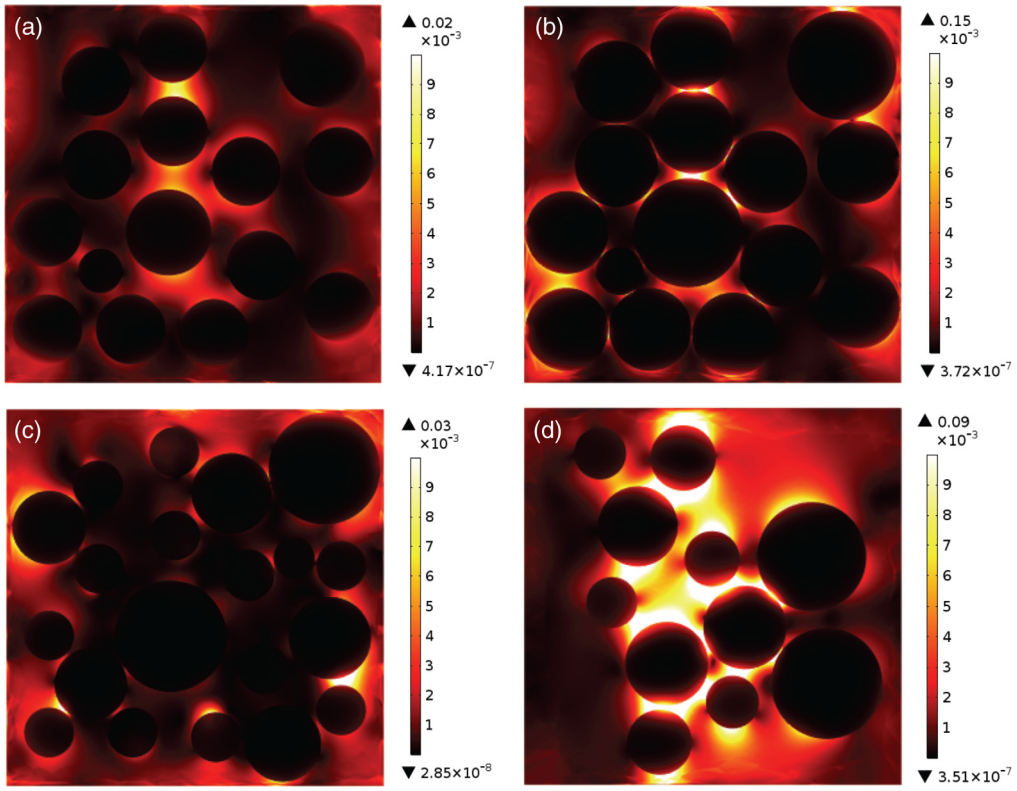

Fig. 7 Time-averaged Poynting vector (W/m^2) on the glass substrate and the air medium of the nanoparticles under $\lambda = 532$ nm, TE (Y-pol.) polarized light at different distances (z) above the glass substrate for standard deviation 12-nm nanoparticle packings: (a) $z = 50$ nm, (b) $z = 100$ nm, (c) $z = 200$ nm, and (d) $z = 400$ nm.

particles. This implies that nanoparticle clustering within the packing can create very high near-field thermal energy transport. In addition, the collective plasmon modes seem to be the strongest between the particles arranged in the packing along the polarization direction of the light. For example, this phenomenon can be observed in the 12-nm standard deviation packing shown in Fig. 7, where the particles aligned in the polarized direction experience very large local field enhancements due to these collective plasmon modes, but those surrounding them, which are not aligned along the direction of field polarization, experience much smaller local field enhancements even though they are a similar size and have similar spacings. This indicates that the collective plasmon modes are best confined between at least three particles clustered along the polarization direction, which results in the energy flux density being ~25 times stronger in the aligned direction than for the other particles at $z = 100$ nm. In addition, it can be observed from Fig. 7(d) that gap plasmon modes, which arise between pairs of closely spaced nanoparticles,[22] can be strong between the particles when the particle spacing is on the order of 10 to 50 nm.

Figure 8 shows the energy flux density for standard deviation 48-nm nanoparticle packings. In this packing, it can be observed that the particles that are much smaller than the mean radius size of 116 nm have started to agglomerate around the larger particles due to attractive vdW forces. These agglomerations result in a less uniform particle distribution than the 12-nm standard deviation case, which results in fewer particles being aligned to the light polarization direction and lower field enhancements. Moreover, larger particles do not create as strong gap modes under laser illumination as smaller particles even if they are aligned along the polarization direction.[12] So, the particles that are much bigger than the mean particle size do not produce strong gap coupling due to the fact that bigger particles tend to scatter much more than they can absorb at 532-nm laser illumination compared to smaller particles.[23] However, it is observed from Fig. 8(c) that particles smaller than the mean radius size adjacent to particles larger than the mean radius size create strong coupling. This implies that only very small nanoparticles

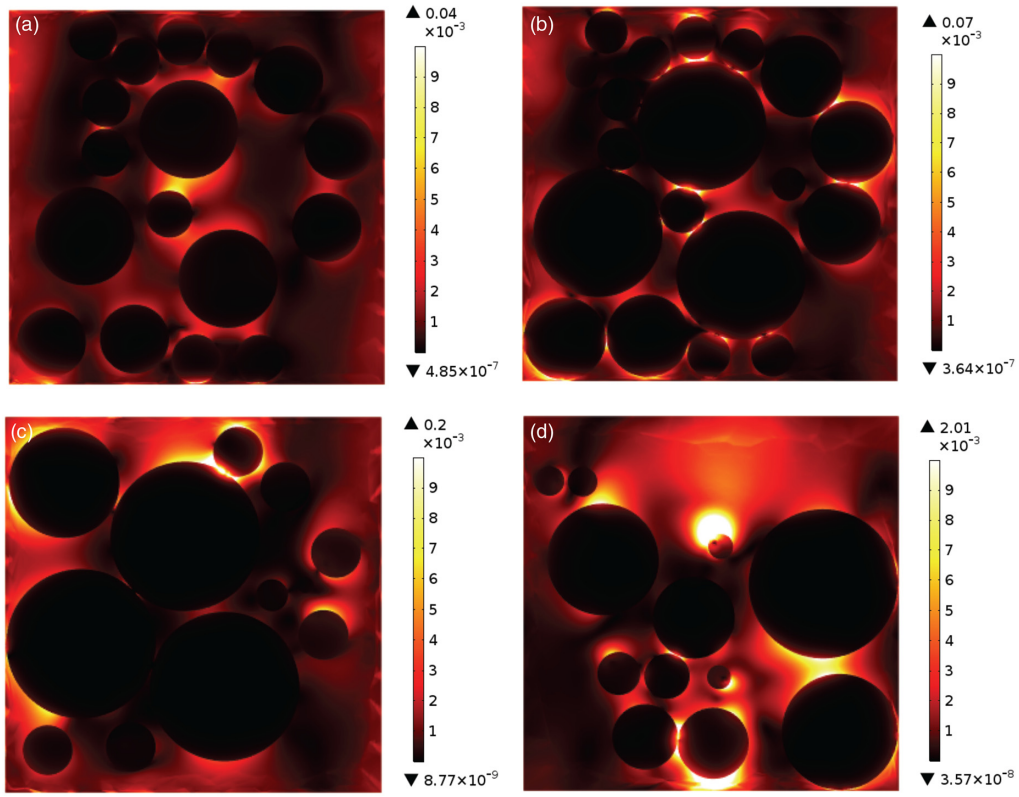

Fig. 8 Time-averaged Poynting vector (W/m^2) on the glass substrate and the air medium of the nanoparticles under $\lambda = 532$ nm, TE (Y-pol.) polarized light at different distances (z) above the glass substrate for standard deviation 48-nm nanoparticle packings: (a) $z = 50$ nm, (b) $z = 100$ nm, (c) $z = 200$ nm, and (d) $z = 400$ nm.

in the agglomeration are contributing significantly to the thermal energy flux generated in the packing.

Figure 9 shows the energy flux density for the 84-nm standard deviation nanoparticle packing. At the top of the packing, the nanoparticles are distributed with a very large spacing but the packing becomes denser for cross-sections closer to the middle of the packing. This is due to the effect of the vdW forces between the particles that results in this type of particle configuration. For the 84-nm standard deviation packing, there are a larger number of very small particles (<50-nm radius), which can create strong plasmonic resonances.[24] However, due to the fact that there are much larger spacings and fewer contact points between the particles in the 84-nm standard deviation case, gap modes are weak and create only weak plasmonic effects between the particles, resulting in nonlocal heat generation around individual nanoparticles. Therefore, due to the spatial arrangements of particles in the 84-nm standard deviation case, there is less overall heat dissipation observed in this packing than in the other nanoparticle packings.

Figure 10 shows the absorption, scattering, and extinction cross-section of the nanoparticle packings as a function of their standard deviations. The extinction cross-section is the summation of absorption and scattering cross-section values. The absorption and scattering cross-section values do not change significantly for the standard deviations between 12 and 48 nm. However, the absorption cross-section starts to decrease and the scattering cross-section starts to increase when nanoparticle standard deviation increases to 84 nm. This is likely due to the large gaps that form in the packings as a result of the increased agglomeration via vdW forces in the high standard deviation packings with more very small and very large particles.

The extinction cross-section also starts to decrease with increasing standard deviation. This implies that optical thickness is higher for the low standard deviation cases. It can also be observed from Figs. 7–9 that the nanoparticles have a higher field intensity when the distance (z)

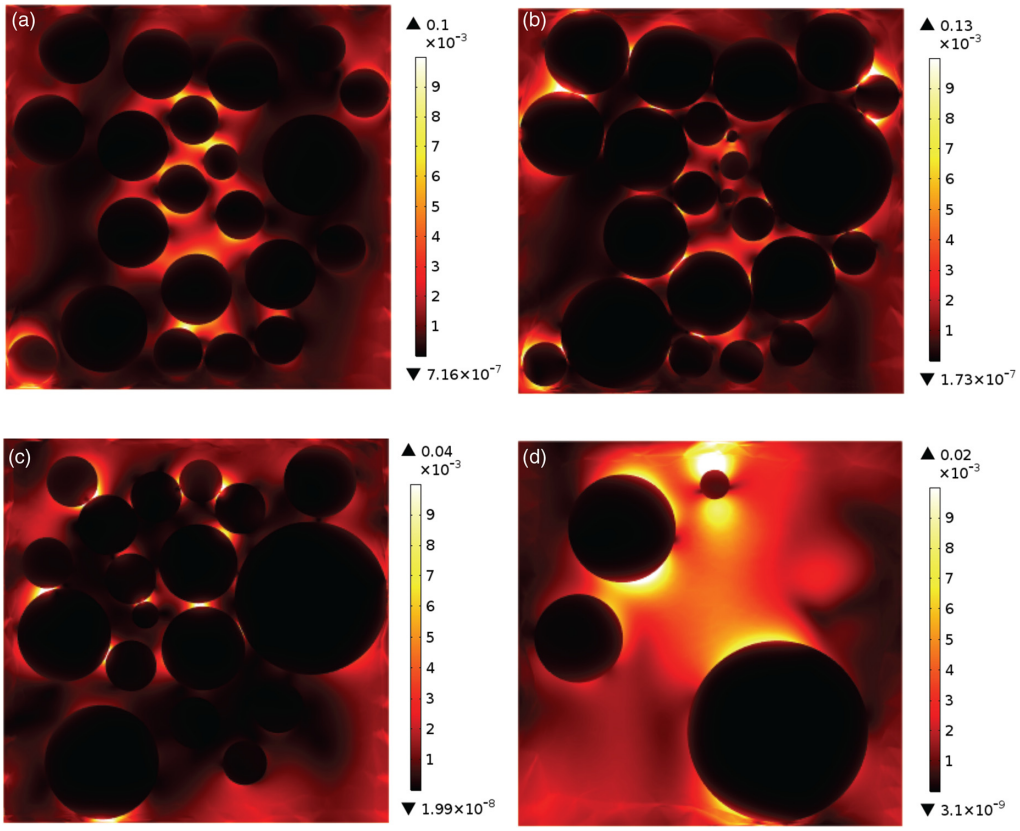

Fig. 9 Time-averaged Poynting vector (W/m^2) on the glass substrate and the air medium of the nanoparticles under $\lambda = 532$ nm, TE (Y-pol.) polarized light at different distances (z) above the glass substrate for standard deviation 84-nm nanoparticle packings: (a) $z = 50$ nm, (b) $z = 100$ nm, (c) $z = 200$ nm, and (d) $z = 400$ nm.

is at 50 nm above the glass substrate for higher standard deviation. This also decreases with decreasing standard deviation, which implies that the light penetrates farther into the nanoparticle packing onto the glass substrate for larger standard deviation than for lower standard deviation. This is likely due to the fact that the nanoparticles are more densely packed in the

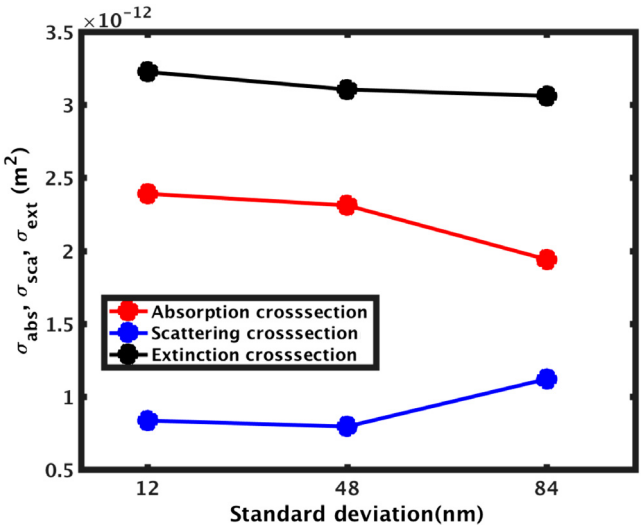

Fig. 10 Absorption, scattering, and extinction cross-section versus particle size standard deviation (nm).

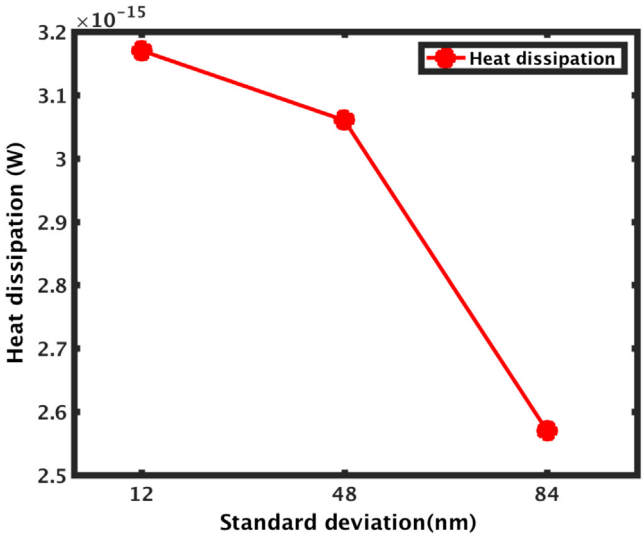

Fig. 11 Heat dissipation (W) versus standard deviation (nm).

smaller standard deviation cases, which results in those packings having higher absorptivities. Indeed, absorption is significantly greater than scattering in these packings and is, therefore, the dominant effect on the extinction cross-section of the packings. This trend starts to change as the particle size standard deviation increases. In other words, the effect of scattering on extinction is getting closer to the effect of absorption on extinction at standard deviation 84 nm than it is for the lower standard deviation cases.

Figure 11 shows the total heat dissipation in the nanoparticle packings, which is found by multiplying the absorption cross-section and the incident laser power, for the three different standard deviations under the 532-nm laser source. Overall, the heat dissipation decreases when the standard deviation of the nanoparticle packings increases. This is due to the fact that particle packings tend to absorb more light for the lower standard deviation cases and have a larger number of contact points between nanoparticles, which results in more heat dissipation within the nanoparticle packing.

The overall results of this study show that wider particle size distributions result in more agglomeration due to the presence of very small nanoparticles that are subject to much larger vdW forces than the average particle. These agglomerations result in a less even distribution of nanoparticles within the packing and larger spacing between particles in the packing. This agglomeration effect also results in fewer contact points between nanoparticles in the packing. Due to these changes in the packing configurations, the packings with wider particle size distributions have less local field enhancements and absorb less light than the packings with narrower particle size distributions. As a result, less heat is dissipated in these packings and the light from the laser source is less efficient at heating the packing. Therefore, in order to sinter the nanoparticles in the packing with the best quality and lowest laser powers, the nanoparticle ink sources used for the μ-SLS system should be designed to have as narrow particle size distribution as possible.

4 Conclusion

This paper has shown that the solutions of Maxwell's equations in frequency domain can be used to analyze the near-field thermal interactions in the nanoparticle packings by examining the packings of nanoparticles that are log-normally distributed in size with different standard deviations. Specifically, it shows that as the standard deviation of the particle size distribution increases, the absorption cross-section and extinction cross-section decrease. Moreover, the heat dissipation from the nanoparticle packings decreases with increasing standard deviation under 532 nm and TE (Y-pol.) laser source, and the penetration depth is higher for higher

standard deviation. This result shows that agglomeration of nanoparticles within the particle packing due to vdW forces can lead to different plasmonic behavior and thermal energy transport under the laser source for similar size packings. These observations are vital steps toward understanding the photonic sintering of nanoparticle packings for subwavelength 3-D electronic interconnects and designing the particle size distributions for these packings in order to maximize sintering quality and efficiency.

References

1. N. Roy, A. Yuksel, and M. Cullinan, "Design and modeling of a microscale selective laser sintering system," in *11th Int. Manufacturing Science and Engineering Conf.*, ASME, pp. V003T08A002–V003T08A002 (2016).
2. C. Chan, J. Mazumder, and M. M. Chen, "A two-dimensional transient model for convection in laser melted pool," *Metall. Trans. A* **15**(12), 2175–2184 (1984).
3. W. Jiang, K. W. Dalgarno, and T. H. C. Childs, "Finite element analysis of residual stresses and deformations in direct metal SLS process," in *Proc. 13th Solid Freeform Fabrication Symp.*, pp. 5–7 (2002).
4. X. Jian and S. Xiaogang, "Simulation and testing of the transient temperature field of infrared laser sintering," *J. Harbin Eng. Univ.* **32**(7), 965–968 (2011).
5. Y. Zhang and A. Faghri, "Melting of a subcooled mixed powder bed with constant heat flux heating," *Int. J. Heat Mass Transfer* **42**(5), 775–788 (1999).
6. X. C. Wang et al., "Direct selective laser sintering of hard metal powders: experimental study and simulation," *Int. J. Adv. Manuf. Technol.* **19**(5), 351–357 (2002).
7. A. V. Gusarov and J. P. Kruth, "Modelling of radiation transfer in metallic powders at laser treatment," *Int. J. Heat Mass Transfer* **48**(16), 3423–3434 (2005).
8. D. Moser et al., "Use of detailed particle melt modeling to calculate effective melt properties for powders," *J. Heat Transfer* **140**(5), 052301 (2018).
9. D. Moser, S. Pannala, and J. Murthy, "Computation of effective thermal conductivity of powders for selective laser sintering simulations," *J. Heat Transfer* **138**(8), 082002 (2016).
10. A. Yuksel, M. Cullinan, and J. Murthy, "The effect of nanoparticle clustering on optoelectronic property," in *Solid Freeform Fabrication Symp.*, pp. 8–10 (2016).
11. A. Yuksel, M. Cullinan, and J. Murthy, "Thermal energy transport below the diffraction limit in close-packed metal nanoparticles," in *Heat Transfer Summer Conf.*, ASME, pp. V002T13A005 (2017).
12. A. Yuksel, M. Cullinan, and J. Murthy, "Polarization effect on out of plane configured nanoparticle packing," in *12th Int. Manufacturing Science and Engineering Conf.*, ASME, pp. V002T01A036 (2017).
13. A. Yuksel et al., "Effect of substrate and nanoparticle spacing on plasmonic enhancement in three-dimensional nanoparticle structures," *J. Micro Nano-Manuf.* **5**(4), 040903 (2017).
14. A. Yuksel and M. Cullinan, "Modeling of nanoparticle agglomeration and powder bed formation in microscale selective laser sintering systems," *Addit. Manuf.* **12**, 204–215 (2016).
15. P. B. Johnson and R. W. Christy, "Optical constants of the noble metals," *Phys. Rev. B* **6**(12), 4370–4379 (1972).
16. J. H. Choi et al., "Thermal conductivity estimation of inkjet-printed silver nanoparticle ink during continuous wave laser sintering," *Int. J. Heat Mass Transfer* **85**, 904–909 (2015).
17. K. An et al., "Selective sintering of metal nanoparticle ink for maskless fabrication of an electrode micropattern using a spatially modulated laser beam by a digital micromirror device," *ACS Appl. Mater. Interfaces* **6**(4), 2786–2790 (2014).
18. A. Yuksel et al., "Analysis of near-field thermal energy transfer within the nanoparticles," *Proc. SPIE* **10346**, 103462X (2017).
19. P. Segovia et al., "Observation of spin and charge collective modes in one-dimensional metallic chains," *Nature* **402**(6761), 504–507 (1999).
20. B. Willingham and S. Link, "Energy transport in metal nanoparticle chains via sub-radiant plasmon modes," *Opt. Express* **19**(7), 6450–6461 (2011).

21. L. A. Sweatlock et al., "Highly confined electromagnetic fields in arrays of strongly coupled Ag nanoparticles," *Phys. Rev. B* **71**(23), 235408 (2005).
22. P. Ginzburg, D. Arbel, and M. Orenstein, "Gap plasmon polariton structure for very efficient microscale-to-nanoscale interfacing," *Opt. Lett.* **31**(22), 3288–3290 (2006).
23. C. F. Bohren and D. R. Huffman, *Absorption and Scattering of Light by Small Particles*, John Wiley and Sons, New York (2008).
24. W. L. Barnes, "Surface plasmon-polariton length scales: a route to sub-wavelength optics," *J. Opt. A* **8**(4), S87–S93 (2006).

Biographies of the authors are not available.